ELSEVIER

Journal of Structural Geology 28 (2006) 1067–1083

JOURNAL OF STRUCTURAL GEOLOGY

www.elsevier.com/locate/jsg

Different stress states in the Burdur–Isparta region (SW Turkey) since Late Miocene times: a reflection of a transient stress regime

Griet Verhaert [a,*], Dominique Similox-Tohon [a], Sara Vandycke [b], Manuel Sintubin [a], Philippe Muchez [a]

[a] *Geodynamics & Geofluids Research Group, Katholieke Universiteit Leuven, Celestijnenlaan 200E, B-3001 Leuven, Belgium*
[b] *Service de Géologie Fondamentale et Appliquée, Faculté Polytechnique de Mons, 9 rue de Houdain, B-7000 Mons, Belgium*

Abstract

The Burdur–Isparta region is a transitional zone between two distinct neotectonic domains in Turkey: the Burdur graben system as the northeastern part of the Fethiye–Burdur fault zone and the Kovada graben at the apex of the Isparta angle. Each domain represents a particular stress regime. Fault data from unconsolidated Pliocene and Quaternary deposits were combined with stress states deduced from pre-Pliocene consolidated rocks in order to reconstruct the stress field evolution in the study area since Late Miocene. Different stress states were identified. They were put in a stratigraphic framework and U/Th dating of fault-related calcite precipitates proved to be an additional tool in constraining the history of the stress states. The reconstructed history reflects a transient stress regime. The evolving stress field indicates that the influence of the Kovada stress regime fades through time and that the influence of the Burdur stress regime is gaining importance, suggesting a northeastwards progression of the Fethiye–Burdur fault zone.

Keywords: Burdur graben; Fethiye–Burdur fault zone; Isparta angle; Kovada graben; Neotectonic; Stress field evolution

1. Introduction

The study area is located at the northwestern apex of the Isparta angle in Turkey (Fig. 1). This structure lies at the boundary between distinct areas of deformation and its tectonic history is important for understanding the geodynamics of this transitional region. The Isparta angle is the link between the Aegean–West Anatolian extensional province bounded to the south by the actively subducting Hellenic arc and the uplifted Anatolian plateau bounded to the south by the Cyprus arc (Glover and Robertson, 1998). The study area, moreover, occupies a particular neotectonic setting, located in between the NE–SW-trending Burdur graben system and the N–S-trending Kovada graben, each representing different stress states. Clarifying the temporal and spatial relationship between these stress states is the main purpose of this paper.

This study focuses on brittle structures, such as joints and faults. Faults were observed in unconsolidated Pliocene and Quaternary deposits, in most cases lacking any kinematic indicators. In the consolidated rocks, on the other hand, kinematic indicators on fault planes allow the sense of fault movement to be deduced. An extensive analysis of faults in consolidated pre-Pliocene deposits was therefore undertaken to combine the fault data where possible, in order to gain a global view of brittle dynamics. Based on the analysis of fault data, different stress states were identified. These stress states were put in a stratigraphic framework to determine a stress state evolution. U/Th dating of a fault-related calcite precipitate and the presence of superimposed slickenlines give additional constraints on this evolution. We postulate that the reconstruction of the history of the stress states, from a synthesis from sites all over the study area, applies to the whole study area and thus reflects a changing stress field through time in the region.

2. Geological setting

The Isparta angle is a triangular-shaped structure, about 120 km long N–S and ca. 50 km wide in the south, extending offshore into the Antalya basin (Fig. 2). The Isparta angle (Blumenthal, 1963) is kinematically linked to the Aegean–West Anatolian extensional province (Fig. 1), through the Fethiye–Burdur fault zone and to the Anatolian plateau through the Sultan Dağ fault. The Isparta angle separates areas of

* Corresponding author. Tel.: +32 16 327798; fax: +32 16 327981.
E-mail address: griet.verhaert@geo.kuleuven.be (G. Verhaert).

0191-8141/$ - see front matter © 2006 Elsevier Ltd. All rights reserved.
doi:10.1016/j.jsg.2006.03.013

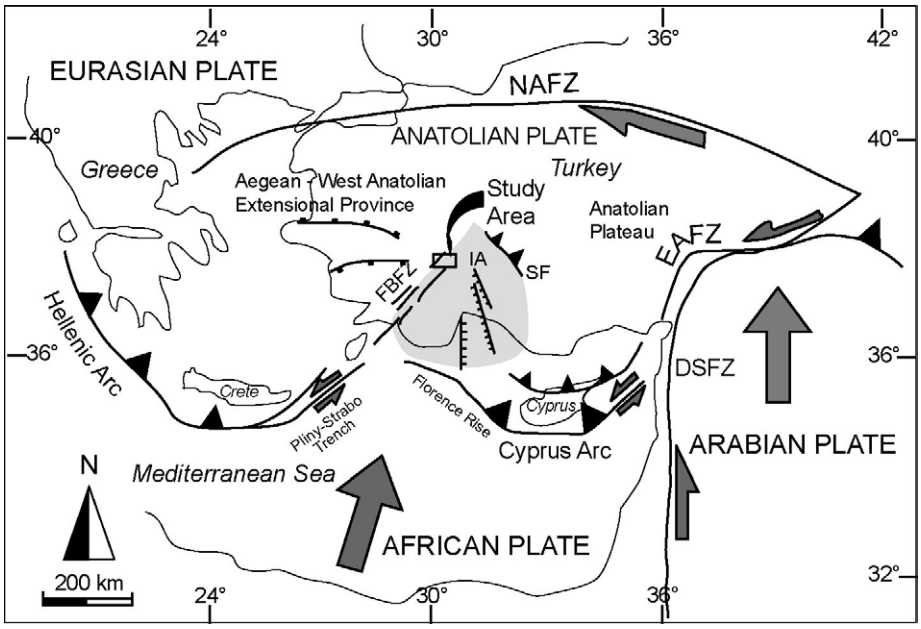

Fig. 1. Schematic tectonic map of the Eastern Mediterranean with indication of the study area. NAFZ: North Anatolian fault zone; EAFZ: East Anatolian fault zone; DSFZ: Dead Sea fault zone; FBFZ: Fethiye-Burdur fault zone; IA: Isparta angle; SF: Sultan Dağ fault.

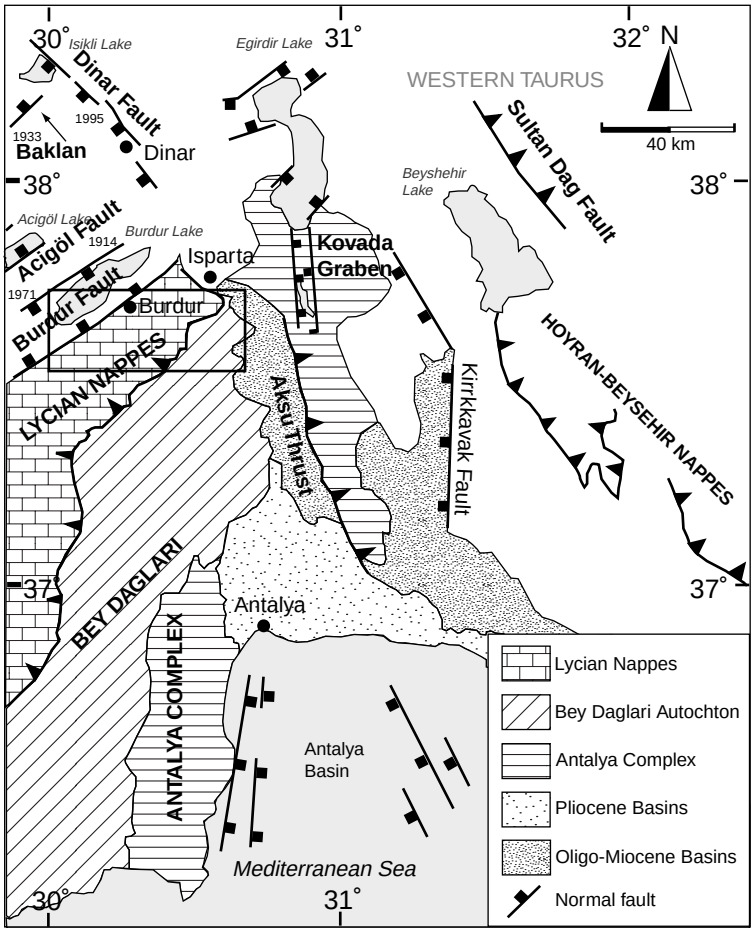

Fig. 2. Location map of the Burdur–Isparta region (modified after Poisson et al., 2003a; Zitter et al., 2003), showing the main neotectonic structural elements. Dates indicate epicentres and dates of major recent earthquakes (Eyidoğan, 1988; Ambraseys and Jackson, 1998; Koral, 2000). The study area is indicated with the black rectangle.

different relative plate motion and distinct deformation. The Anatolian plateau is uplifting and moves westwards (Glover and Robertson, 1998). The Aegean–West Anatolian extensional province has a southwestward displacement and a counterclockwise rotation (Glover and Robertson, 1998). To the south, the Isparta angle is, according to Zitter et al. (2003), a key link with the African plate boundary between the Hellenic and the Cyprus arcs. Both arcs are characterized by back-arc extension (Glover and Robertson, 1998).

The Isparta angle also reflects Miocene convergent tectonics (Fig. 2), whereby the autochthonous Bey Dağlari massif was overthrusted by several nappes (i.e. Antalya complex, Lycian nappe and Hoyran Beyşehir nappe; e.g. Poisson et al., 2003b; Robertson et al., 2003). The Middle–Late Miocene and Pliocene correspond to a change of the kinematics in the Isparta angle (Poisson et al., 2003b). The Aksu regime of compression was characterized by translation from E to W, dated as post-Tortonian and pre-Pliocene and a translation from NE to SW, dated as Late Miocene in the south of the Isparta angle (Poisson, 1977; Frizon de Lamotte et al., 1995; Poisson et al., 2003a). Palaeomagnetic data indicate that no detectable rotation of the core of the Isparta angle took place during Plio-Quaternary time (Kissel and Poisson, 1986).

Neotectonics in this region are dominated by an extensional regime that started in Late Miocene–Early Pliocene times (~5 Ma BP; Şengör et al., 1985; Bozkurt, 2001). The Burdur area is characterized by three NE–SW-trending half-grabens, bounded to the southeast by major NW-dipping, slightly listric, basement faults, the Burdur, Acigöl and Baklan faults (Fig. 2; Price and Scott, 1994). Quaternary basins developed within these grabens, occupying the central part of wider, fault-bounded Pliocene basins (Price and Scott, 1991). To the northeast this graben system terminates against the NW–SE-trending Dinar fault. The Burdur graben system represents a stress regime dominated by biaxial NW–SE and NE–SW extension, i.e. the Burdur stress regime. The Burdur graben is interpreted as the northeastern part of the Fethiye–Burdur fault zone, which is developing from the SW to the NE and is currently interpreted as the landward continuation of the Pliny–Strabo trench (ten Veen and Kleinspehn, 2002; ten Veen, 2004). The Burdur area is situated in a zone of significant weak to moderate seismic activity in recent and historical times. The recent earthquake record concerns two quakes on the Baklan fault (1925: Ms 6.0; 1933: Ms 5.8), two quakes on the Burdur fault (1914: Ms 7.1; 1971: Ms 6.2) and one quake on the Dinar fault (1995: Ms 6.1) (see Barka et al., 1995; Eyidoğan and Barka, 1996; Koral, 2000). The neotectonic

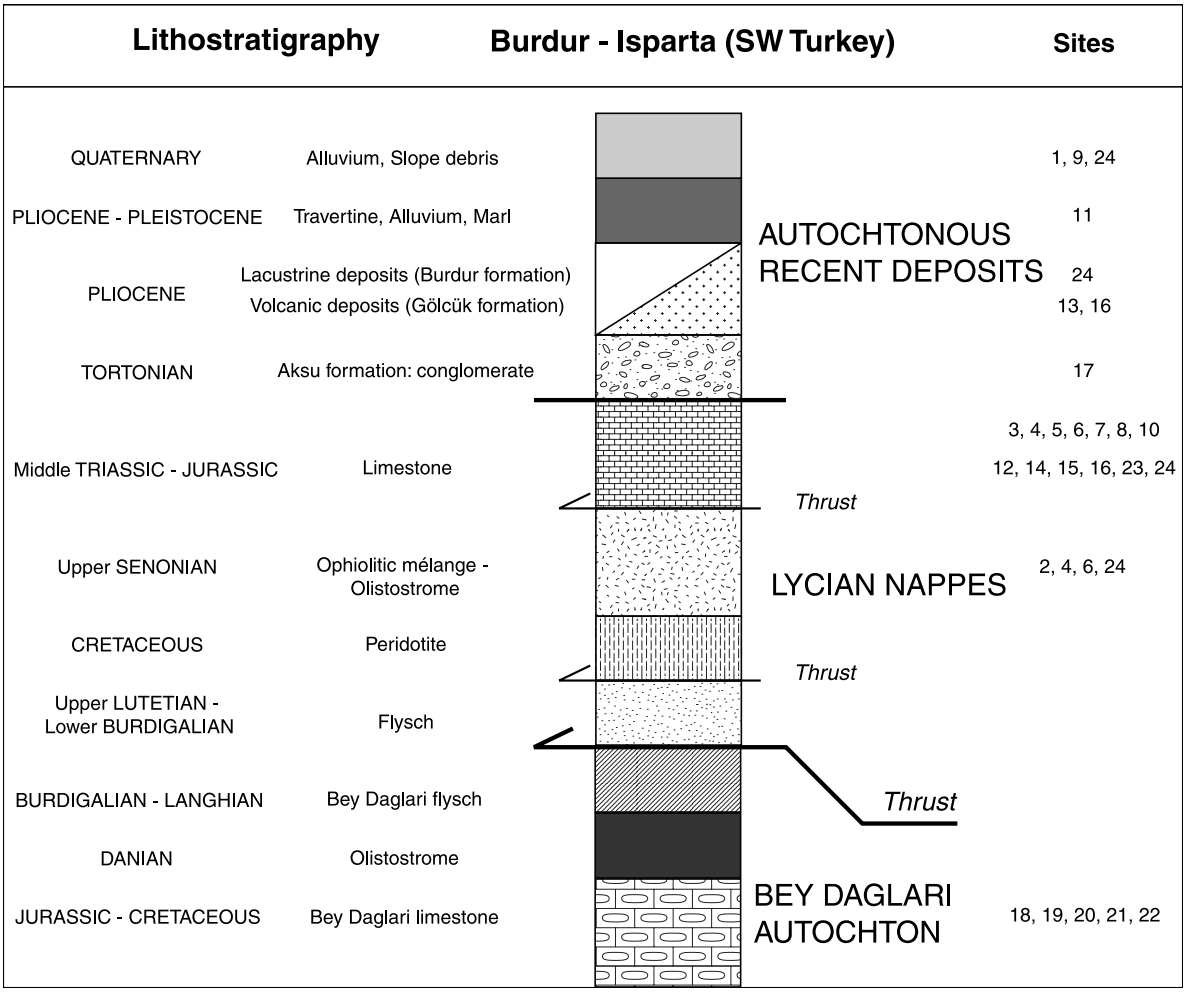

Fig. 3. Lithostratigraphy and structural relationships of the different lithologies in the study area (after Şenel, 1997) with indication of sites.

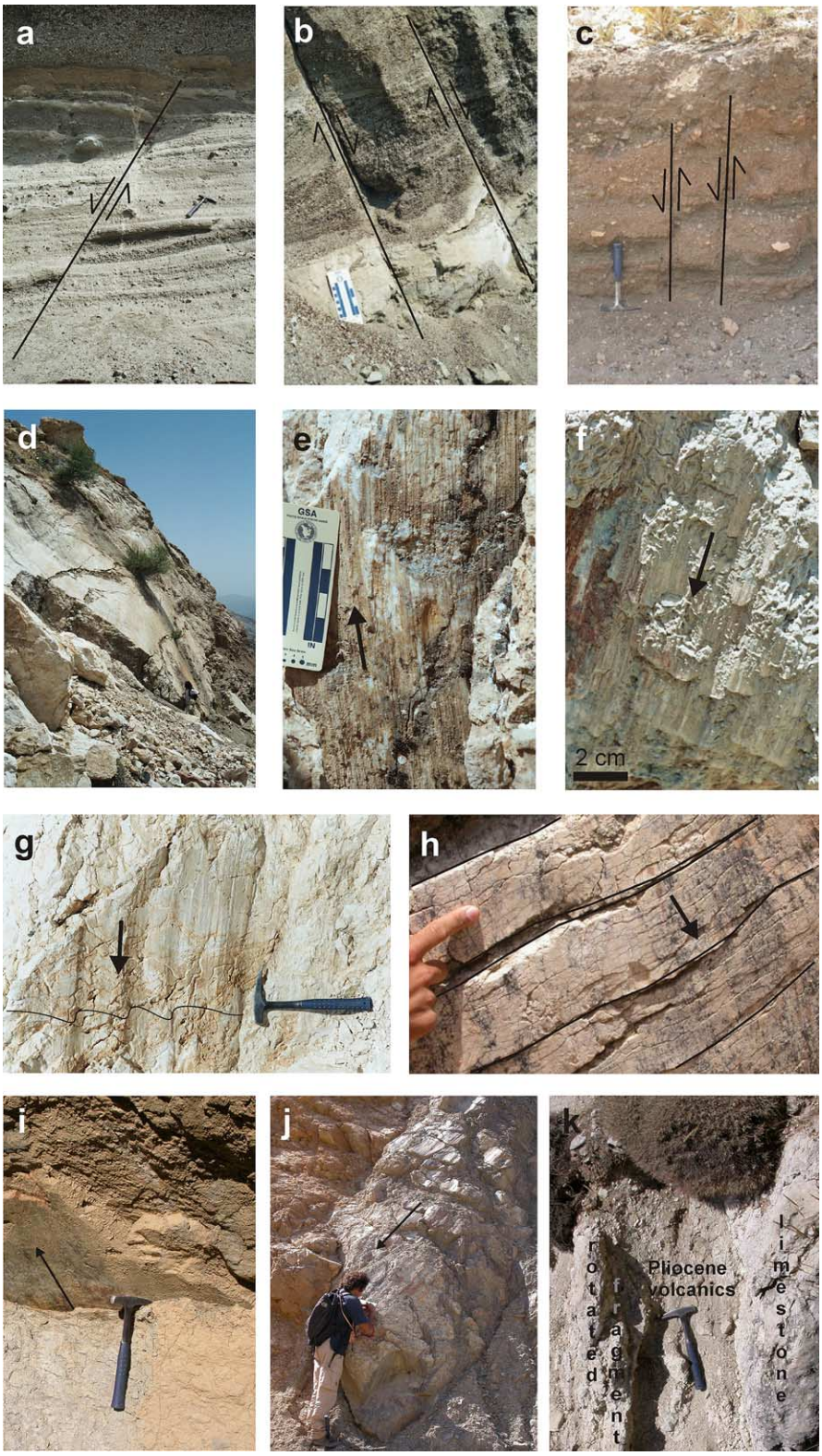

Fig. 4. Examples of brittle structures in the lithologies of the study area: (a) normal fault in Pliocene volcanic tuff (site 13; hammer is 33 cm); (b) normal faults in Quaternary alluvium (site 24; scale bar is 10 cm); (c) normal faults in recent colluvium (~100 a BP; site 9); (d) fault plane in limestone substrate (site 8; person is 1.75 m); (e) slickensides and slickensteps on a limestone fault plane in the hanging wall (arrow indicates fault movement; site 7; scale bar is 10 cm); (f) slickensides and slickensteps in Tortonian conglomerates (arrow indicates fault movement; site 17); (g) corrugations on a normal fault plane in limestone are characterized by sinusoidal profiles normal to their length axes, slip movement is parallel to the length axes (arrow; site 23); (h) comb fractures intersecting a normal fault plane, normal to slip movement (arrow; site 10; finger is 8 cm); (i) striations on the hanging wall of a fault plane in Pliocene andesite rocks with indication of fault movement (site 16); (j) slickensides on a fault plane in Pliocene andesite rocks (site 16; person is 1.75 m); (k) fault at the contact between limestone and Pliocene volcanics, fragments are brecciated limestone are reoriented within the volcanics (site 16).

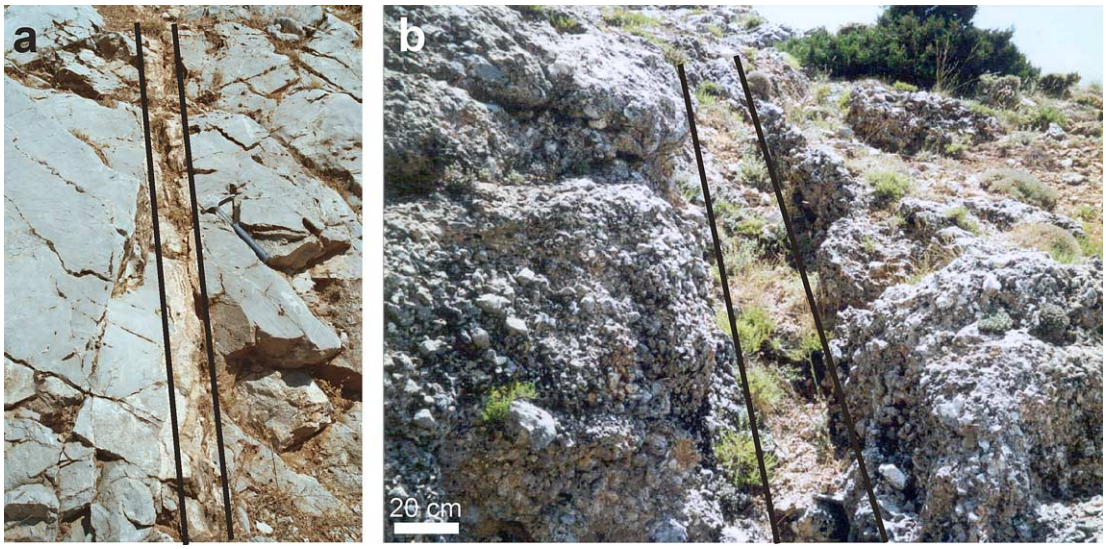

Fig. 5. (a) Vein, filled with crustiform calcite precipitates and joints crosscutting the limestone (site 22; hammer is 33 cm); (b) joint crosscutting scree deposits (site 1).

setting of the apex of the Isparta angle (east of Isparta city) is dominated by the N–S-trending Kovada graben and subparallel lineaments (Glover and Robertson, 1998). The Kovada graben is 25 km long by 2–3 km wide, running southwards from Eğirdir lake, with the small Kovada lake filling the southern end of the graben. Subordinate Quaternary N–S fault lineaments mapped to the E of Kovada graben extend over more than 20 km (Glover and Robertson, 1998). This graben system represents a stress regime dominated by E–W extension, i.e. the Kovada stress regime. The east of the Isparta angle comprises two major structures, the Late Miocene Aksu thrust and the Kirrkkavak fault. The Kirrkkavak fault is a prominent fault lineament, running ca. 90 km northwards from the Mediterranean and then bending to NW–SE. The fault experienced a phase of right-lateral displacement during Miocene time and developed into dominantly normal faulting during Pliocene time (Glover and Robertson, 1998).

The stratigraphic and lithological units that occupy the study area range from Triassic to Holocene age (Fig. 3). Jurassic–Cenomanian limestones of the Bey Dağlari massif occupy a large part of the region. Middle Triassic–Lower Jurassic (Lias) limestones and Upper Senonian ophiolitic mélange and olistostromes of the Lycian nappes are present. On the lower slopes towards the valleys flysch deposits crop out belonging to the Miocene Aksu basin that developed as a foreland basin in front of the proceeding Lycian nappes (Collins and Robertson, 1998). The Miocene Aksu basin was filled by coarse Tortonian conglomerates, several kilometers thick (Poisson et al., 2003b). Pliocene Gölçük volcanic deposits, 4.5 Ma old (Price and Scott, 1991; Yağmurlu et al., 1997) overlie the Lycian limestones in the north of the study area. Pliocene lacustrine deposits (Burdur formation) are present near Burdur Lake. Conglomerates of Pliocene age are present at Gravgaz (site 23). Important Holocene tufa deposits are present in the alluvial plane of Başköy valley (9000–600 a BP; Vermoere et al., 1999). The entire region is characterized by voluminous Late Tertiary and Quaternary scree deposits (Librecht et al., 2000). Also recent colluvium ($\sim$100 a BP) is present.

3. Brittle tectonic features

This study focuses on brittle structures, such as joints and faults. Fault movement was observed in unconsolidated deposits by displacement of distinct layers in Pliocene volcanic tuff deposits (Fig. 4a), Pliocene lacustrine deposits, Quaternary alluvium (Fig. 4b), Pleistocene slope deposits and Holocene colluvium (Fig. 4c). No displacement sense could be deduced in these unconsolidated deposits from slickensides, slickensteps, or other kinematic indicators. Most of the fault planes crosscutting these post-Miocene deposits have, however, very representative meter-scale fault planes with clear (normal) displacement of distinct layers despite their lack of kinematic indicators. They therefore clearly represent important fault activity. The fault data of the unconsolidated deposits and consolidated rocks in the study area are combined in the discussion where possible, in order to gain a global view of brittle dynamics. Consequently, fault movement was reconstructed by measuring slickenlines and slickensteps on fault planes in the consolidated rocks such as limestone (Fig. 4d and e), ophiolitic mélange and Tortonian conglomerates (Fig. 4f) and Pliocene andesite deposits. Moreover particular kinematic indicators on normal faults—such as corrugations (Fig. 4g) and comb fractures (Fig. 4h)—characteristic of Aegean-type normal faults in limestone substrates (Hancock and Barka, 1987) were used to determine fault movement. Slickensides were also measured in Pliocene andesite (Fig. 4i–k).

Many joints, most of which occur in the limestone substrate, have been observed and measured. Some of the joints (up to 50 cm wide) are filled by crustiform calcites and can be described as veins (Verhaert et al., 2004) (Fig. 5a). Fig. 5b shows a joint crosscutting scree deposits. No evidence of propagation structures, e.g. plume structures and Riedel shears, could be observed since most of them are filled with calcite.

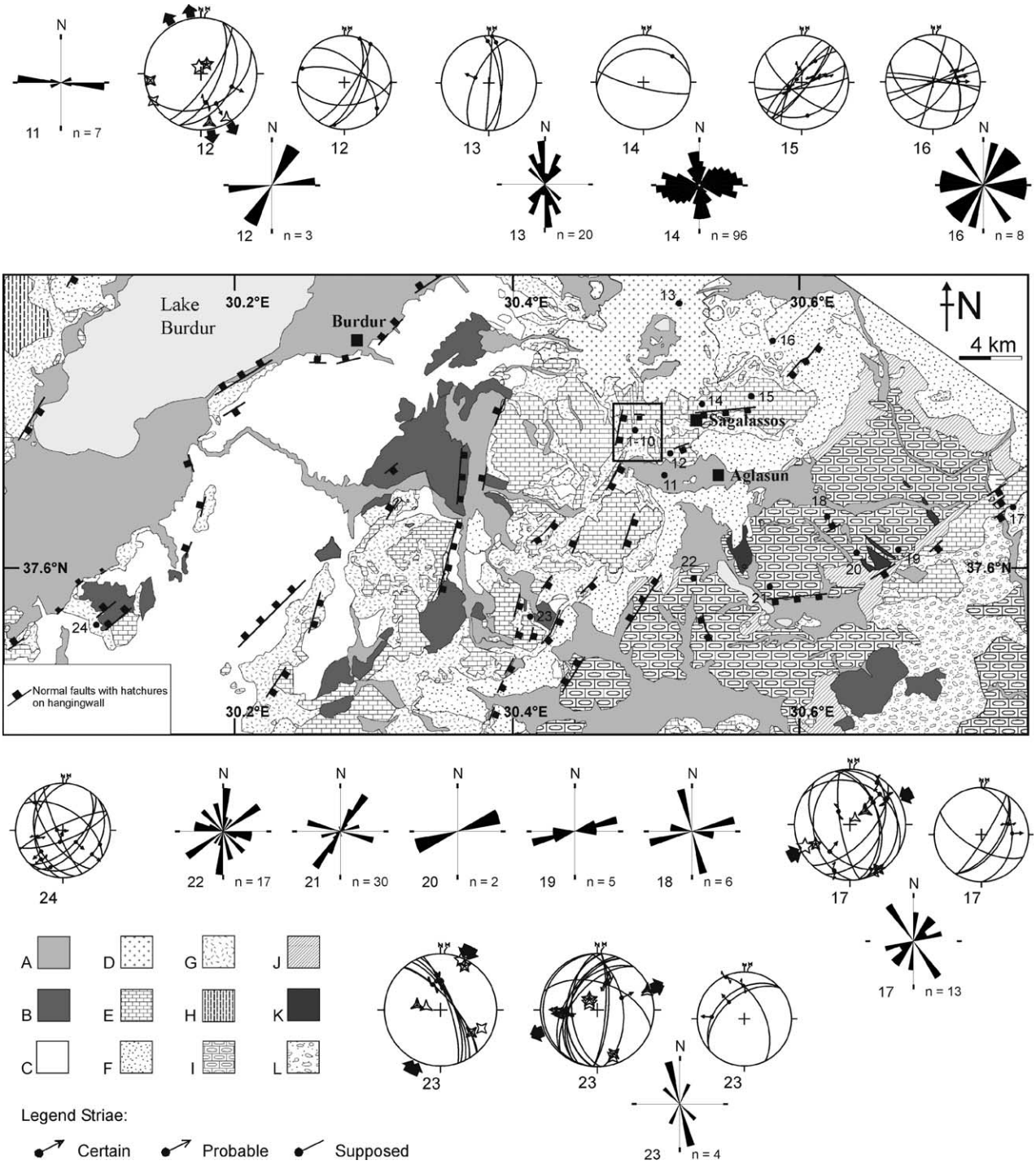

Fig. 6. Geometry and palaeostress tensors of the fault data in sites 11–24. For each site, the fault data are plotted on a lower-hemisphere equal-area projection and subdivided into large stereoplots with populations for which a palaeostress tensor could be calculated and small stereoplots with the other fault data that were insufficiently abundant to calculate a reliable stress tensor. The principal palaeostress axes (σ_1, σ_2 and σ_3) are represented by open and crossed 5-, 4- and 3-point stars for the INVDIR and R4DT methods, respectively (Angelier, 1984, 1990) and main extension/compression (black arrows) are indicated for each fault population. Relative sizes of the 5-, 4- and 3-point stars are indicative of Φ value. Stress tensor values are given in Tables 1 and 2. Sites are located on a simplified geological map of the study area with indication of Fig. 7 (modified after Şenel, 1997). Legend: (A) Quaternary deposits (alluvium and slope deposits); (B) Pleistocene–Pliocene deposits (tufa, old alluvial fan, marl); (C) Pliocene lacustrine deposits (Burdur formation); (D) Pliocene volcanic deposits (Gölcük formation); (E) Middle Triassic–Jurassic Lycian limestone; (F) Upper Lutetian–Lower Burdigalian flysch (Lycian nappes); (G) Upper Senonian ophiolitic mélange and olistostrome unit (Lycian nappes); (H) Cretaceous peridotite (Lycian nappes); (I) Jurassic–Cretaceous Bey Dağlari limestone; (J) Burdigalian–Langhian flysch (Bey Dağlari massif); (K) Danian olistostrome (Bey Dağlari massif); (L) Tortonian conglomerates (Aksu formation). The geometry of the joint data are also shown (maximum percentage: 9%; mean percentage: 5.5%; standard deviation: 2.54%; vector mean: 84.49°; confidence interval 7.22%; R-mag: 0.63.

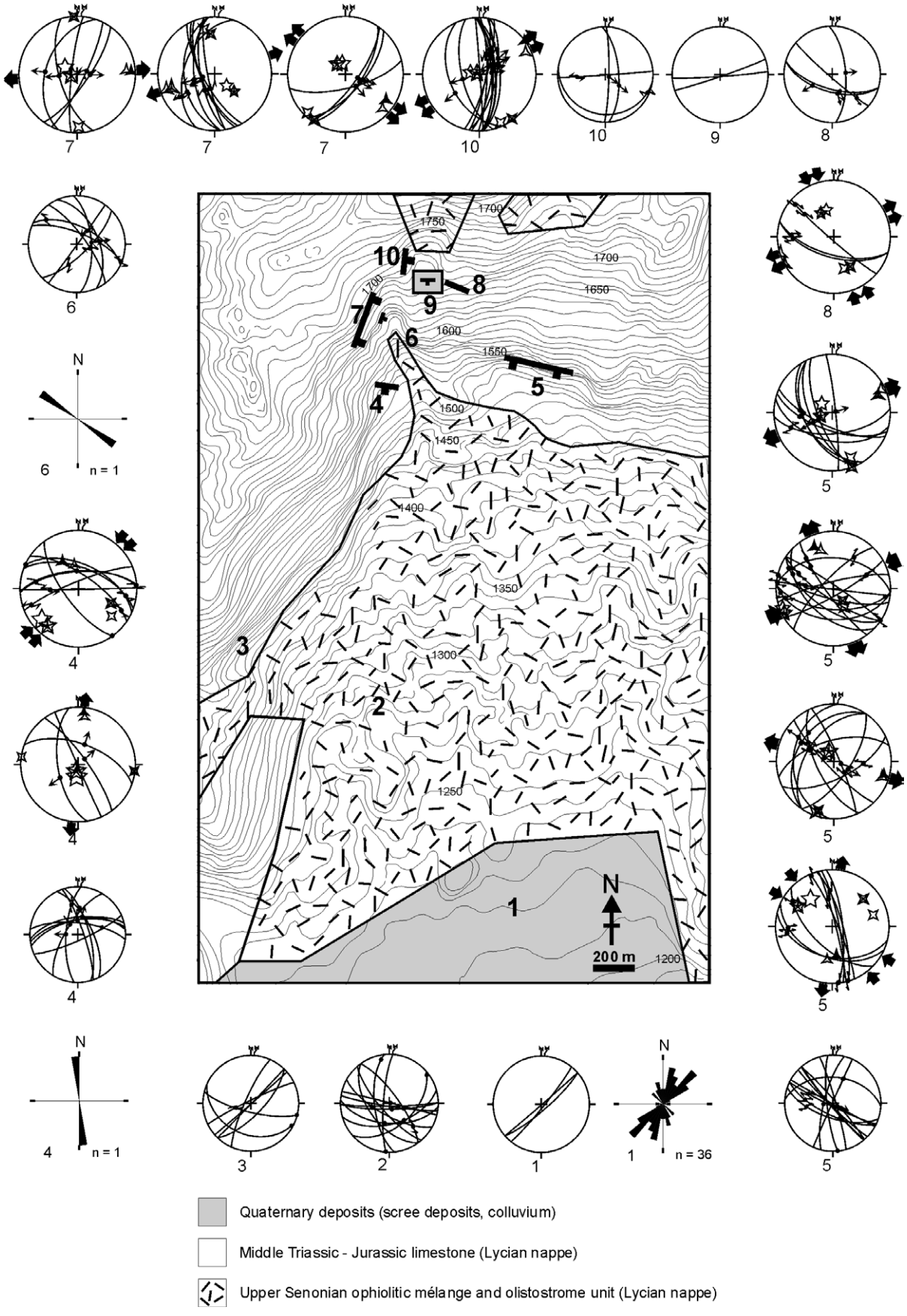

Fig. 7. Geometry and palaeostress tensor of the fault data in the Sarikaya area (sites 1–10). Geological map modified after Şenel (1997). Legend of diagrams as for Fig. 6.

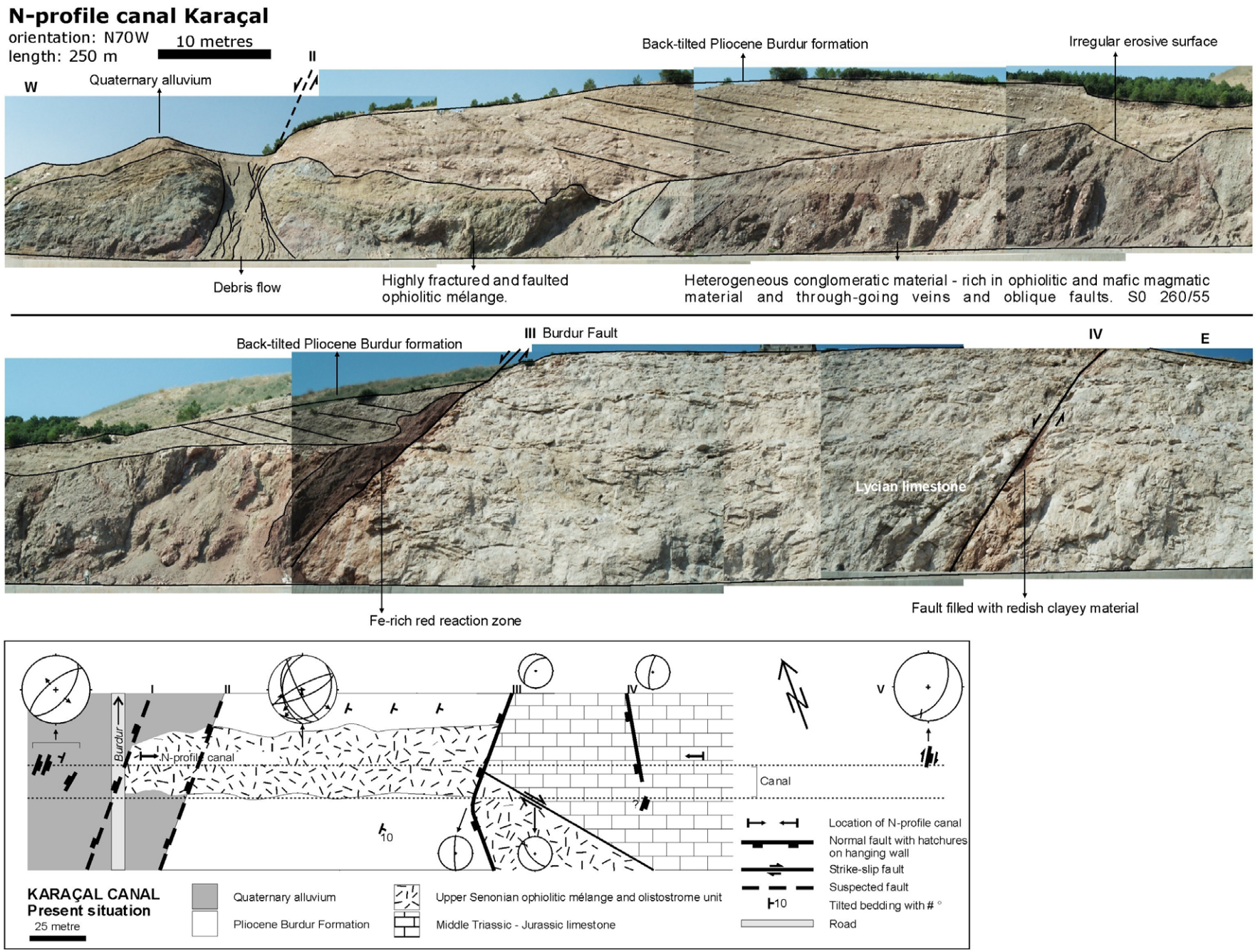

Fig. 8. Northern profile of Karaçal (site 24) with indication of fault data and geological map of the Karaçal area with indication of fault data. Legend of diagrams as for Fig. 6.

It was therefore impossible to decide whether they are tensional or hybrid joints. After the opening of the joints, superficial meteoric waters infiltrated the open joints. During the descent of the meteoric waters, columnar calcite precipitated in the joints, forming speleothems (Verhaert et al., 2004). The fabric of the joint-filling calcites is not tectonically related and can therefore not be used to determine the opening sense.

In a detailed field survey on 24 sites, joint orientations ($n=234$) and fault data ($n=267$) affecting a wide range of lithologies were gathered. The orientation data are given in azimuth convention (right-hand rule): strike direction/dip and pitch of slickensides in degrees from strike of fault (right-hand rule). The fault data are plotted on a lower-hemisphere equal-area projection for each site and subdivided into populations for which a palaeostress tensor ($n\geq 4$) could be calculated. Procedures for this subdivision are explained in Section 4 below. Stereoplots are presented for the remaining faults that belong to (several) other populations and for which no tensor could be calculated ($n<4$) (Figs. 6–8). The Sarikaya complex occupies an area 1 km by 800 m, characterized by seven geomorphologically different fault zones (Fig. 7): wedge-shaped faults (site 4); one large striated fault plane (site 5); several small fault planes in a gully (site 6); cohesive intensely fractured limestone with multiple slip planes (site 7); an undulating fault plane (site 8); faults crosscutting Holocene colluvium (site 9); and non-cohesive limestone fault breccias crosscut by several parallel fault zones (site 10). All sites, except 1 and 9 have pre-Pliocene deposits. At Karaçal (site 24; Fig. 8) two profiles, which crosscut the seismogenic Burdur fault (1914: Ms 7.1; 1971: Ms 6.2) were studied in detail in an excavated canal bed. In this site a range of lithologies is present. They comprise a Middle Triassic–Jurassic limestone bedrock and the Senonian ophiolitic mélange and olistostrome unit. Pliocene lacustrine Burdur formation and Quaternary alluvium are deposited in the western part of the profiles.

First, the sites with post-Miocene deposits are described in detail. Then, the Tortonian conglomerates are described and finally the faults crosscutting the pre-Miocene deposits are briefly discussed.

At site 13 (Pliocene volcanic tuff and andesite deposits), four faults trending N–S have been recorded. One has a normal movement with a displacement of ~50 cm (Fig. 4a) and three faults have a strike-slip movement, as shown by slickensteps in andesite volcanic deposits but with unknown sense of displacement.

At site 16 (Pliocene volcanic deposits) nine faults have been recorded. Two NW–SE-trending normal faults dipping to the east, with pitch of 74S and 81S are present in Pliocene andesite rocks (Fig. 4i). One conjugate fault (120/45S) and one fault with 20/90 orientation, at the contact between flysch and volcanics are observed. Also one fault with orientation 40/63S is observed with a pitch of 50N (Fig. 4j). Four ENE–WSW-trending faults are located at the contact between limestone and volcanics. They display fault movement after deposition of the Pliocene volcanics, since fragments of brecciated limestone are located and reoriented within the volcanics, close to the fault contact (Fig. 4k). They reveal, however, no sense of fault movement.

The Quaternary consolidated screes (site 1) are crosscut by NE–SW-trending faults ($n=3$). These faults displace the consolidated screes by more than 10 cm due to a normal fault movement. No kinematic indicators of fault movement were detected.

Recent Holocene colluvium (site 9) is characterized by several nearly parallel E–W- and ENE–WSW-trending faults ($n=10$). These faults displace the colluvium down dip (displacement 10–20 cm) (Fig. 4c). Due to their unconsolidated nature, no sense of fault movement could be observed, so no tensor could be calculated.

At Karaçal (site 24; Fig. 8), two NE–SW-trending fault steps (faults I and II) were detected. The first fault step (fault I) crosscuts the Quaternary alluvium and a height difference of several meters is observed. The second fault step (fault II) is a topographical step between the Pliocene Burdur formation to the east and Quaternary alluvium to the west. The Pliocene Burdur formation is intensely back-tilted. In the Quaternary alluvium, synthetically and antithetically NE–SW-trending normal faults are present ($n=3$; orientations: 230/70 and 40/60). NW–SE- to N–S-trending conjugate reverse faults principally affect the Tortonian conglomerates (site 17; Fig. 4f). The limestone and ophiolitic mélange also show reverse faulting (sites 4, 5, 23 and 24).

Normal faults are omnipresent in the Middle Triassic–Cenomanian aged limestone (sites 3–8, 10, 12, 14, 15, 23 and 24) and in the Senonian ophiolitic mélange (sites 2 and 4). Strike-slip faults are also detected in the Triassic–Cenomanian limestone and Senonian ophiolitic bedrock (sites 2, 3, 5, 6, 8, 10, 15 and 24).

At Gravgaz (site 23), normal faults (~200/50 pitch 70) crosscut limestone and Pliocene conglomerates.

Site 10 comprises multiple N–S-trending normal slip planes and zone-parallel layers of fault breccia. The fault planes contain oblique to dip slip corrugations, comb fractures and slickensides. The damage zone of this fault zone is composed of non-cohesive limestone breccias, crosscut by several parallel faults, defining an incohesive breccia belt, typical of shallow, active normal faults crosscutting limestone substrate in the Aegean region (Stewart and Hancock, 1991).

At Karaçal (site 24), in the northern profile (Fig. 8), two faults crosscut the limestone (31/51 pitch 155 (fault V) and 190/75 (fault IV)). One fault separates the limestone and the ophiolitic mélange (220/50; fault III). The Pliocene Burdur formation lies on top of the ophiolitic mélange and is intensely back-tilted at this fault plane. Both the Burdur formation and the ophiolitic mélange are characterized by an iron-rich red alteration zone at the contact with the fault plane. The ophiolitic mélange itself is intensely fractured and several normal and reverse faults could be detected. In the southern profile, a dextral fault plane displaces the ophiolitic mélange relative to the limestone (140/65 pitch 160). Another fault plane (180/85) displaces the Pliocene Burdur formation relative to the ophiolitic mélange and olistostrome unit.

Several joint orientations were measured in the area. Figs. 6 and 7 show joint data measured in 15 sites. N–S-, E–W-, NE–SW- and NW–SE-trending joints are obvious. At site 14, structural

analysis of the Sagalassos fault (a WSW–ENE-trending active normal fault composed of three right-lateral overstepping fault sections, indicating a sinistral component of movement) by Sintubin et al. (2003) shows that deformation in the exposed footwall block is characterized by conjugate systems of vertical to near-vertical fractures, trending normal and parallel to the master fault. They represent the near-surface shatter zone, which formed during the initial blind faulting at depth, typical of active normal fault zones cutting bedrock carbonates within the Aegean region (Stewart and Hancock, 1990).

4. Palaeostress analysis

The fault-slip data collected suggest a complex history of faulting and reactivation. Taking into account the previous data concerning the affected lithologies, the chronology of different faults and their respective fault movement ($n=116$), fault populations were determined in order to separate conjugate Andersonian fault systems in each site. These fault populations consist of strike-slip, normal or reverse faults. In searches for the best stress tensor to fit these faults, numerical methods were used that automatically minimize one parameter, i.e. the sum of the angular misfits. This angular misfit, i.e. the difference between the theoretical slickenlines predicted from some trial tensor and the real slickenlines, was used to separate fitting and non-fitting faults (e.g. Liesa and Lisle, 2004). The remaining non-fitting faults were used to search for other tensors by repeating the procedure. Although these inversion methods are automatic, the separation of heterogeneous fault data into different fault populations was carried out manually, so that these procedures for separating the stress tensors should be considered as semiautomatic. Methods that use this approach are those proposed by Etchecopar et al. (1981), Armijo et al. (1982) and Angelier (1984) amongst others. The direct inversion method (INVDIR program, Angelier, 1990) was used in this study. It consists of determining the best-fitting reduced palaeostress tensor for a given fault slip data set, identifying the attitude of the three principal stress axes (maximum, intermediate and minimum stress: σ_1, σ_2 and σ_3, respectively) and the ratio $\Phi=(\sigma_2-\sigma_3)/(\sigma_1-\sigma_3)$ of principal stress magnitudes. A second numerical method was used to calculate the respective palaeostress tensors: the R4DT iterative search method of Angelier (1984). This method also implies the determination of stress axes in four dimensions as well as the ratio Φ. In this iterative search, a function is adopted that minimizes the slickenline-shear angle only, so that permutations of axes may occur for special data sets (discussed in Angelier, 1984, p. 5841). Both results are shown in Figs. 6 and 7, with σ_1, σ_2 and σ_3 represented by open and crossed 5-, 4- and 3-point stars for the INVDIR and R4DT methods, respectively. It is clear from Figs. 6 and 7 and Tables 1 and 2 that both numerical methods lead to similar stress tensors.

At Sarikaya (Fig. 7; Tables 1 and 2) the dominant stress states are: a NE–SW compression (site 4); two wrench regimes with an ENE–WSW compression and NNW–SSE extension (site 5) and with a NNW–SSE compression and ENE–WSW extension (site 5), respectively; a NE–SW extension (sites 4, 5, 7, 8 and 10); NW–SE extension (sites 5 and 7) and an E–W

Table 1
Palaeostress tensor computations with the semiautomatic INVDIR method (Angelier, 1984) based on fault slip data in different lithologies. The columns contain from left to right: NF: number of fault slip data with sense of movement; trend and plunge of the principal stress axes (in degrees); Φ=ratio $(\sigma_2-\sigma_3)/(\sigma_1-\sigma_3)$; Coh (%): Coherence between the data; α: average angle between computed shear stress and observed fault slip data (in degrees); RUP (%): values below 50% indicate good fits between actual fault slip data and computed shear distributions

Site	Longitude (E)	Latitude (N)	NF	σ_1	σ_2	σ_3	Φ	Coh (%)	RUP (%)	α (°)	Stress
Middle Triassic–Liassic limestone—Upper Senonian ophiolitic mélange and olistostrome unit—Jurassic–Cenomanian limestone											
4	30.4736	37.6687	9	230/19	129/27	350/56	0.082	100	40	15	NE–SW compression
4	30.4736	37.6687	5	187/72	278/0	8/18	0.041	100	30	8	NE–SW extension
5	30.4785	37.6689	4	311/71	158/17	65/8	0.493	100	50	16	NW–SE extension
5	30.4785	37.6689	8	315/76	200/6	108/13	0.380	100	43	18	NE–SW extension
5	30.4785	37.6689	10	249/6	149/59	342/30	0.433	90	43	15	ENE–WSW compression, NNW–SSE extension
5	30.4785	37.6689	8	322/38	74/26	189/41	0.168	100	45	20	NNW–SSE compression, NNE–SSW extension
7	30.4731	37.6704	4	343/75	225/7	133/14	0.319	100	13	3	NW–SE extension
7	30.4731	37.6704	14	135/66	346/21	252/11	0.627	100	21	3	NE–SW extension
7	30.4731	37.6704	5	301/70	178/11	85/16	0.298	100	36	9	E–W extension
8	30.4757	37.6712	4	344/49	162/41	253/1	0.612	100	23	7	ENE–WSW extension, NNW–SSE compression
10	30.4743	37.6718	11	282/77	156/8	65/10	0.409	100	26	10	NE–SW extension
12	30.5001	37.6623	6	346/80	240/3	150/10	0.462	100	22	7	NW–SE extension
23	30.4061	37.5687	13	312/75	162/13	70/7	0.414	100	27	7	NE–SW extension
23	30.4061	37.5687	6	23/4	114/21	283/69	0.528	100	15	1	NNE–SSW compression
Tortonian conglomerates											
17	30.7408	37.6317	9	244/11	153/5	38/78	0.337	89	40	21	NE–SW compression

Table 2
Palaeostress tensor computations with the semiautomatic R4DT method (Angelier, 1984) based on fault slip data in different lithologies. The columns contain from left to right: NF: number of fault slip data with sense of movement; trend and plunge of the principal stress axes (in degrees); Φ = ratio $(\sigma_2-\sigma_3)/(\sigma_1-\sigma_3)$; Coh (%): Coherence between the data; α: average angle between computed shear stress and observed fault slip data (in degrees); RUP (%): values below 50% indicate good fits between actual fault slip data and computed shear distributions

Site	Longitude (E)	Latitude (N)	NF	σ_1	σ_2	σ_3	Φ	Coh (%)	RUP (%)	α (°)	Stress
Middle Triassic–Liassic limestone—Upper Senonian ophiolitic mélange and olistostrome unit—Jurassic–Cenomanian limestone											
4	30.4736	37.6687	9	254/11	157/32	1/56	0.193	82	71	35	NE–SW compression
4	30.4736	37.6687	5	187/73	97/0	7/17	0.065	100	30	7	NE–SW extension
5	30.4785	37.6689	4	334/74	197/11	105/10	0.209	100	46	9	NW–SE extension
5	30.4785	37.6689	8	254/74	160/1	70/16	0.459	100	56	11	NE–SW extension
5	30.4785	37.6689	10	244/5	142/68	335/21	0.359	100	46	12	ENE–WSW compression, NNW–SSE extension
5	30.4785	37.6689	8	301/30	48/27	172/47	0.342	100	50	18	NNW–SSE compression, NNE–SSW extension
7	30.4731	37.6704	4	321/71	214/6	123/18	0.359	100	9	2	NW–SE extension
7	30.4731	37.6704	14	132/52	354/30	252/21	0.791	100	19	3	NE–SW extension
7	30.4731	37.6704	5	264/82	357/0	87/8	0.176	100	44	1	E–W extension
8	30.4757	37.6712	4	331/50	151/40	241/0	0.691	100	25	7	ENE–WSW extension, NNW–SSE compression
10	30.4743	37.6718	11	297/86	144/3	54/2	0.209	100	38	9	NE–SW extension
12	30.5001	37.6623	6	31/73	262/10	170/13	0.592	100	36	2	NW–SE extension
23	30.4061	37.5687	13	324/71	159/18	68/5	0.392	100	30	5	NE–SW extension
23	30.4061	37.5687	6	29/11	126/33	282/55	0.558	100	5	0	NNE–SSW compression
Tortonian conglomerates											
17	30.7408	37.6317	9	240/29	147/6	48/60	0.658	89	49	24	NE–SW compression

extension (site 7). As shown in Tables 1 and 2, site 5 has quite large α-values for the NE–SW extension ($\alpha = 18°$) and the wrenching with NNW–SSE compression and ENE–WSW extension ($\alpha = 20°$). Numerical experiments suggest, however, that only the significance of palaeostress results that yield average deviation angles from 25° or more should be questioned (Ramsay and Lisle, 2000).

The remaining sites with Middle Triassic–Cenomanian limestone (Fig. 6; Tables 1 and 2) are characterized by a NW–SE extension (site 12) and NE–SW extension (site 23). At site 23, this NE–SW extension moreover affects Pliocene conglomerates. Also a NE–SW compression with NW–SE-trending dextral strike-slip faults is observed at site 23. The Tortonian conglomerates (site 17) are dominantly influenced by a NE–SW compression. This stress state has a high α-value (21°) and a low coherence. This is most likely the result of the heterogeneous nature of the conglomerate.

5. History of stress states

Since no stress tensor based on brittle fault data in the unconsolidated Pliocene and Quaternary deposits could be deduced, these data were compared with the stress states that could be calculated from the pre-Pliocene consolidated rocks. The different identified stress states can be placed relatively in time by putting them in a stratigraphical framework. However, the combination of the palaeostress tensors of the pre-Pliocene deposits with the fault data of the Pliocene and Quaternary deposits requires the following assumptions: (a) the stress state was homogeneous in the whole region and (b) all the similar faults, independently of their location and geological context, represent the same stress tensor. Moreover, the aim of this study is to frame this stress field evolution in a regional tectonic context and to deduce the main geodynamic influence of the neighbouring tectonic domains. The integration concerns a large area, so that side-effects are as far as possible neglected and a global view can be obtained. U/Th dating gives an additional strength to this procedure by dating a striated calcite coating on a fault plane in limestone bedrock (Verhaert et al., 2004). The separation between the different tectonic events has been established mainly based on lithostratigraphical evidence.

5.1. Dating and chronology by lithostratigraphical records

Evidence for the chronology of tectonic events is obtained by the relative ages of the stratigraphical units affected by the different populations.

At site 5, a wrenching stress state with a NNW–SSE compression and NNE–SSW extension is observed in the limestones. At site 8, on a parallel fault plane, strike-slip faults, originating from a NNW–SSE compression and ENE–WSW extension stress state are present. These sites, 400 m apart, both represent strike-slip faults on parallel fault zones in the same lithology. A NNW–SSE compression is therefore present and gives rise to strike-slip faults in the limestone substrate.

Site 5 showed a palaeostress tensor for wrenching with an ENE–WSW compression and NNW–SSE extension. In several other sites, strike-slip faults that fit in this stress state,

crosscutting Triassic–Cenomanian limestone (sites 3, 6, 8, 10 and 12) and ophiolitic mélange (site 2), were observed.

The NE–SW compression stress state is observed in the Triassic–Cenomanian limestone (sites 5 and 23) and in the ophiolitic mélange (sites 4 and 24). It is also present in the Tortonian conglomerates (site 17), implying an activity during the Late Miocene.

An E–W extension is observed in Triassic–Cenomanian limestone (sites 4–8 and 15), ophiolitic mélange (site 4) and Tortonian conglomerates (site 17). Also in site 13, an E–W extension was present, responsible for the N–S-trending normal fault, implying activity at least until the Pliocene.

The NE–SW extension is observed in Triassic–Cenomanian limestone (sites 3–7, 10, 15 and 23), ophiolitic mélange (sites 2, 4 and 24), Tortonian conglomerates (site 17), Pliocene volcanic deposits (site 16) and Pliocene conglomerates (site 23). This stress state thus implies impact at least until the Pliocene.

NW–SE extension stress states and linked faults are present in the Triassic–Cenomanian limestone (sites 3–5, 7, 10, 12, 15 and 23), ophiolitic mélange (sites 2 and 4), Tortonian conglomerates (site 17), Pliocene volcanic deposits (site 16), Quaternary consolidated screes (site 1) and in Quaternary alluvium (site 24). At Karaçal (site 24), after deposition of the Pliocene Burdur formation, a NW–SE extension causes normal displacement and the back-tilting of this lacustrine formation. In the Quaternary deposits, this NW–SE extension is responsible for the faults and probably for the two fault steps in the topography. These data suggest that the NW–SE extension was active until at least the Quaternary.

Several faults that originated from a NNW–SSE extension are observed in Triassic–Cenomanian limestone (sites 4, 8, 12, 14 and 15), ophiolitic mélange (sites 2 and 4) and Pliocene volcanic deposits (site 16). Holocene recent colluvium ($\sim$100 a; site 9) showed several ENE–WSW- to E–W-trending normal faults, resulting from the NNW–SSE extension. This stress state was certainly active until very recent.

5.2. Chronology by using superimposed slickenlines

Another chronological argument is the presence of superimposed slickenlines, indicating activation of the fault during multiple tectonic events. At site 7, the fault plane (195/45) shows superimposed slickenlines, implying a reactivation of a fault, originating in an E–W extension (195/45W pitch 80S) in a NE–SW extension (195/45W pitch 46S). At site 8, a large undulating fault plane in limestone bedrock is present (see Fig. 4d). This undulating fault plane has an orientation between 110/60 and 138/85 and slickenlines with pitches of 12W, 29W, 34W and 35W and dextral fault movement. These fault data originated in the wrench regime with a NNW–SSE compression and an ENE–WSW extension. One striation, on the fault plane with orientation 135/85 has a pitch of 30E. This fault movement corresponds to the wrench regime with an ENE–WSW compression and a NNW–SSE extension. This probably indicates a contemporary occurrence of these two populations since the 30E striation is pre- and post-dated by fault movements with pitches of 12W and 35W, respectively, deduced from superimposed slickenlines. On the fault plane a breccia is present composed of ophiolitic and limestone fragments. This breccia is cemented and covered by a thick flowstone. The flowstone shows several striations with average orientation 110/60 and normal fault movement with pitch 70E. These fault data are the result of the NNW–SSE extension. At site 4, slickenlines on a fault plane (286/60) with pitch 158 and sinistral movement are superimposed by slickenlines with pitch 89. This indicates a reactivation of the ENE–WSW compression in a NE–SW extension. At site 5, reverse fault movement (270/45 pitch 104) has been superimposed by sinistral strike-slip faulting (270/45 pitch 3). Reverse faulting with a NE–SW direction of compression is therefore post-dated by the wrenching with an ENE–WSW compression direction.

5.3. Knowledge from U/Th dating

In a study of the origin of palaeofluids in a normal fault setting, calcite filling joints and striated calcite coatings on fault planes were dated with U/Th dating techniques (Verhaert et al., 2004). This calcite precipitated from fluids with a relatively deep origin (>1 km) and calcite coatings were pre- and post-dated by fault movements, indicating that calcite precipitation was linked with fault activity. Dating of these calcite coatings gives a maximum age of the subsequent fault movement, responsible for the striations on the calcites, thus helping to identify the impact period of certain stress states.

The oldest calcite cement associated with the 110/70 fault at site 5 occurs in the thin veins in the damage zone and its age is $\sim$472 ka. Striated calcite precipitates (slickensides with a pitch of 54°) on a fault plane (110/70, NE–SW extension, site 5) have an age of 199 ± 38 ka. Hence, the reactivation of this normal fault (NE–SW extension) in a NW–SE extension occurred not more than 200 ka ago since the calcite coating predates this fault movement. Calcite precipitating in cavities made by the slickensteps on this fault plane has an age of 18 ± 2.7 ka. A flowstone on the 286/60 fault plane at site 4 (NE–SW extension) gives an age of 17.7 ± 2.5 ka. At sites 4 and 5, no fault movement has taken place since deposition of the calcite in the cavities of slickensteps and since deposition of the flowstone.

6. Discussion

6.1. Stress field evolution

Different stress states have been identified and placed relatively in time (Fig. 9). U/Th dating of a fault-related calcite precipitate gives an additional constraint and the results from the superimposed slickenlines agree with the chronological evidence based on lithostratigraphy. We postulate that the reconstruction of the history of the stress states, from a synthesis from sites all over the study area, applies to the whole study area and thus reflects a changing stress field through time in the region.

Two wrench stress states were observed in pre-Miocene deposits. Superimposed slickenlines reflect a multidirectional

transition between them. A NE–SW compression affects Tortonian conglomerates, indicating activity at least until the Late Miocene. Subsequently, E–W extension, affecting Pliocene deposits, suggests activity at least until the Pliocene. The NE–SW extension occurred until the Pliocene. The NW–SE extension has certainly been active until the Quaternary. The U/Th dating of a fault-related calcite coating, which predated a fault movement in a NW–SE extension stress state, indicates an impact of this stress state later than 200 ka BP. The NNW–SSE extension was active until the Holocene, affecting colluvium of ~100 a BP.

6.2. Swapping and rotation of stress axes

The transition between the two wrench stress states can be caused by a swapping of σ_1 and σ_3 (Angelier and Bergerat, 1983). On the contrary, the σ_1 direction remained almost the same during the switch to the Late Miocene compression. In Pliocene time, an extension stress regime was present, expressed by an E–W and NE–SW extension stress state. The evolution between these two extensions was caused by a rotation of σ_2 and σ_3. The shift to the NW–SE extension could have been the result from the swapping of σ_2 and σ_3. After a rotation of σ_2 and σ_3, a NNW–SSE extension was present in the study area.

The swapping and rotation of σ_2 and σ_3 during the extension stress regime could have occurred several times. The type of stress regime where σ_1 is vertical and σ_2 approaches σ_3 is usually designated as radial or multidirectional extension (Armijo, 1977). This type of tectonic stress is common in intraplate zones that have undergone slight to moderate extensional tectonic movement, frequently accompanied by

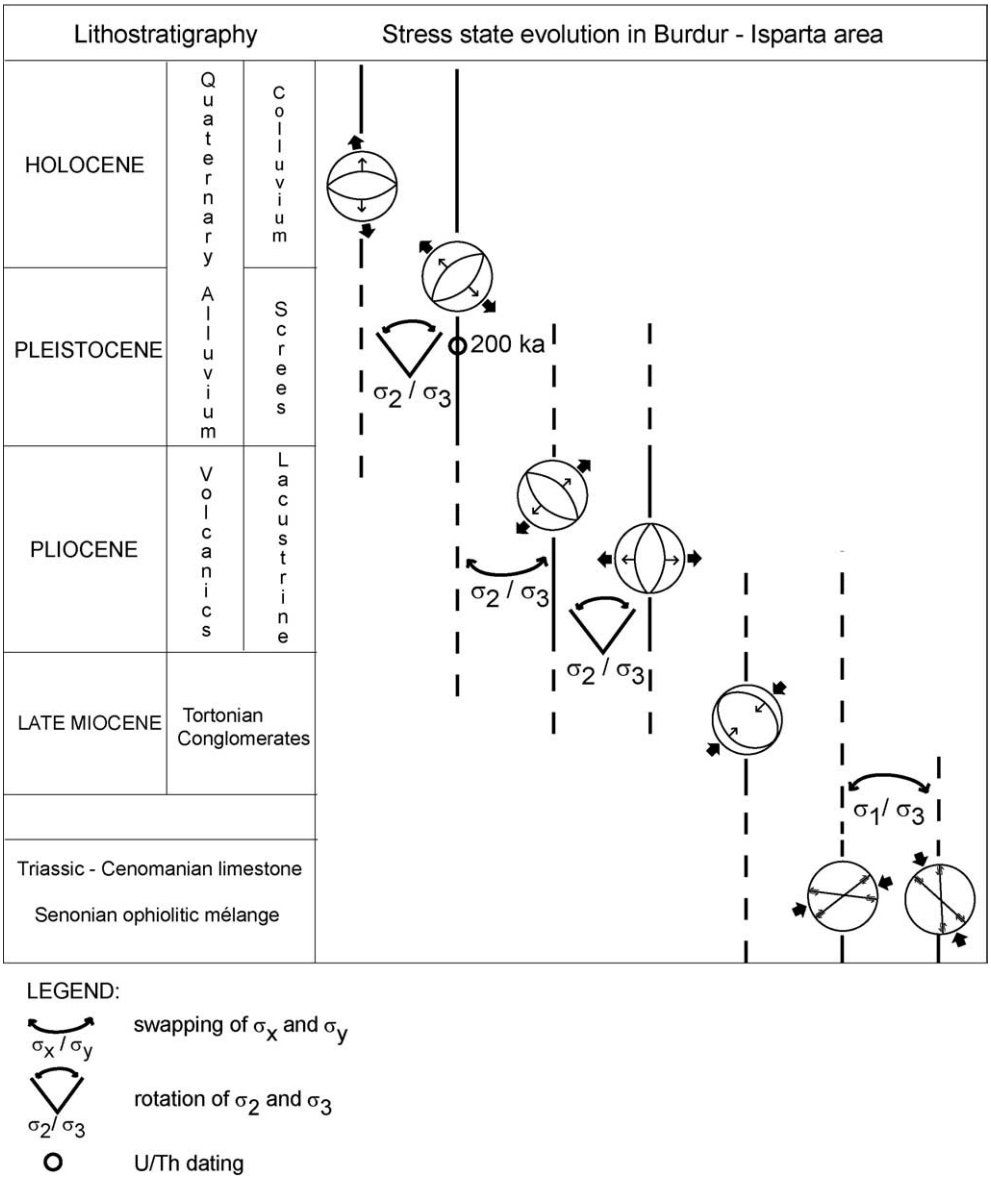

Fig. 9. Palaeostress state evolution recorded from the Late Miocene to recent times in the Burdur–Isparta region. The diagrams represent schematic fault systems and average stress axes directions for each stress state. Black vertical lines indicate impact period of the stress state. Chronology is deduced from lithostratigraphy and U/Th dating of a fault-related calcite precipitate.

vertical uplift (Hancock et al., 1987; Arlegui-Crespo and Simón-Gómez, 1998). In some cases, multidirectional extension gives rise to systematic conjugate normal faults, following either one or two orthogonal strikes. However, they very often show a high directional variability (Arlegui-Crespo and Simón-Gómez, 1998). Spatial variation of the orientation of main stress axes is therefore an important phenomenon especially in extensional settings where stress trajectories can rotate due to previous discontinuities. A frequent phenomenon here is the swapping of σ_2 and σ_3 stress axes.

From Miocene to Pliocene the stress regime changed from compression to extension. At site 7, superimposed slickenlines imply the transition of an E–W extension to a NE–SW extension (195/45W pitch 46S). This clearly indicates a changing stress field.

6.3. Geodynamic evolution

The combination of the palaeostress tensors of the pre-Pliocene deposits with the fault data of the Pliocene and Quaternary deposits made it possible to reconstruct the history of stress states. This eventually enables us to infer a stress field evolution in the study area since we assume that the reconstruction of the history of stress states applies to the whole study area and thus reflects a changing stress field through time. In this particular plate tectonic setting, the stress field changed from wrenching via compression to extension. For the wrench stress states no neotectonic significance could yet be identified. In order to check the neotectonic influence of the neighbouring domains and to reveal the origin of the stress field, this stress field evolution is framed within the published tectonic history of the Aegean–West Anatolian extensional province (Figs. 10 and 11). In Late Miocene time (Fig. 10a) the Burdur graben system experienced a NE–SW extension (Temiz et al., 1997). The Isparta angle is under compression, related to the SW-trending Aksu thrust. The Aksu thrust was dated as post-Tortonian and pre-Early Pliocene, since the recent units affected by thrusting were believed to be Tortonian conglomerates (Poisson et al., 2003a). The study area was also under the influence of this Aksu regime during the Late Miocene and no extension was present. Moreover, the NE–SW compression and the wrenching with the ENE–WSW compression were

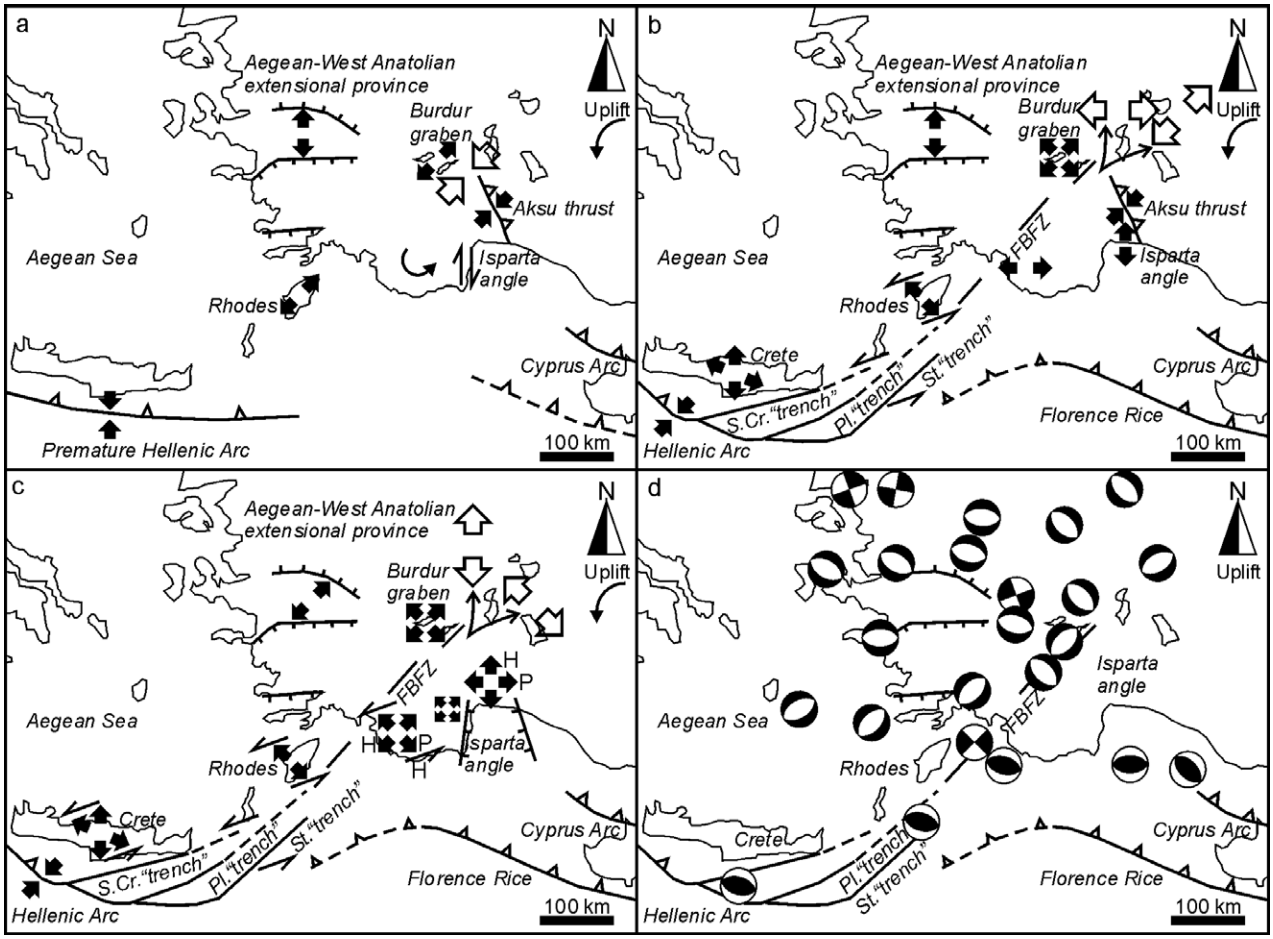

Fig. 10. Geodynamic evolution of SW Turkey and the Aegean area from the Late Miocene to recent times with indication of the dominant stress regimes. Geodynamic setting during (a) Late Miocene; (b) during the Pliocene; and (c) in Pleistocene (P) and Holocene (H) times; (d) recent earthquakes and focal plane mechanisms (Ms > 5.5). Black arrows indicate published stress regimes (McKenzie, 1978; Jackson and McKenzie, 1984; Taymaz and Price, 1992; Zanchi and Angelier, 1993; Price and Scott, 1994; Barka et al., 1995; Eyidoğan and Barka, 1996; Temiz et al., 1997; Glover and Robertson, 1998; Papazachos, 1999; Mantovani et al., 2000; Hançer and Karaman, 2001; Temiz et al., 2001; ten Veen and Kleinspehn, 2002; Emre et al., 2003; Poisson et al., 2003a; Robertson et al., 2003; Peterek and Schwarze, 2004; ten Veen, 2004) and open arrows indicate stress states deduced from this study.

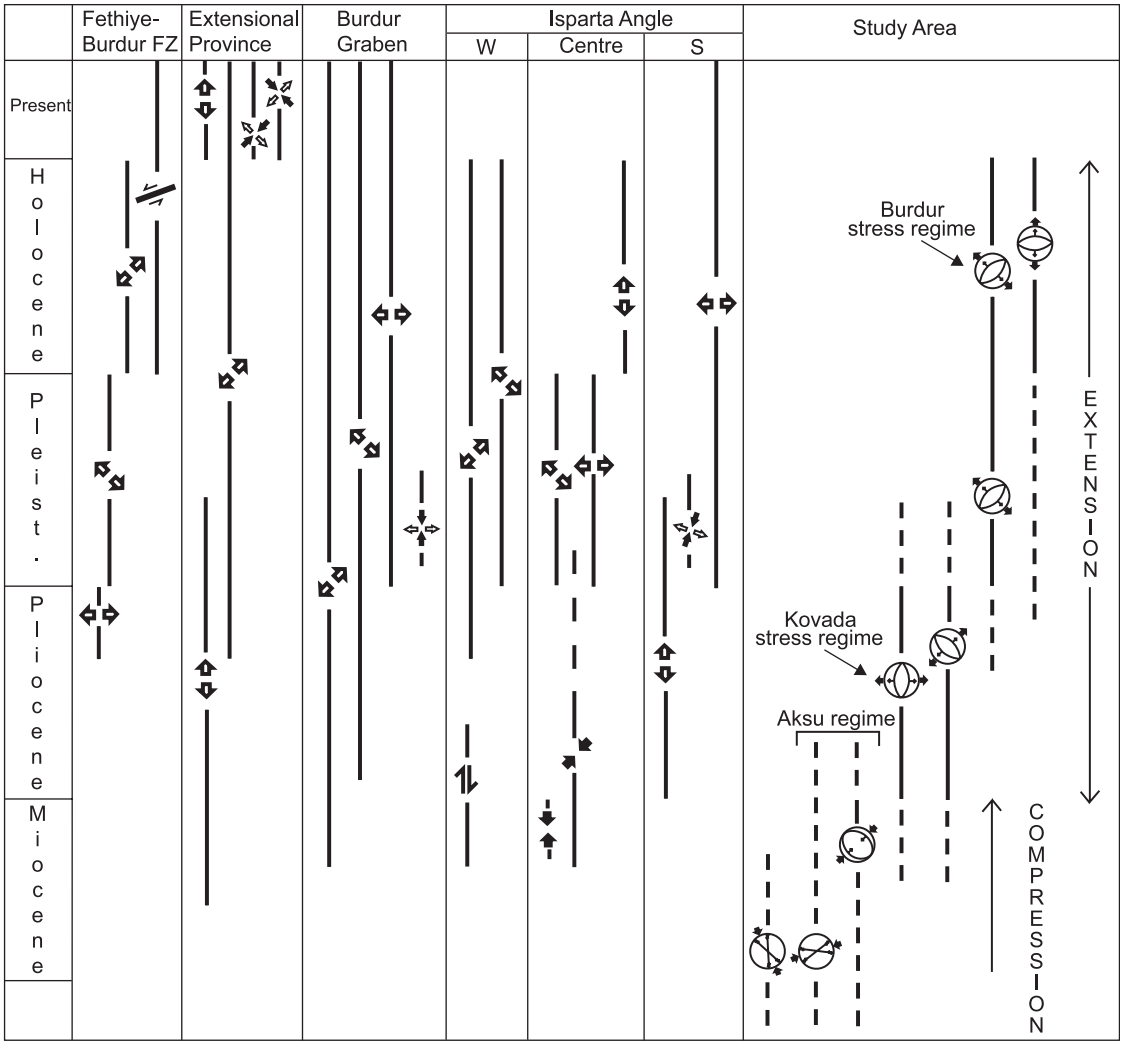

Fig. 11. Stress field evolution recorded from the Late Miocene to recent times in the different main neotectonic domains in SW Turkey according to different authors and current study (after McKenzie, 1978; Jackson and McKenzie, 1984; Taymaz and Price, 1992; Zanchi and Angelier, 1993; Price and Scott, 1994; Barka et al., 1995; Eyidoğan and Barka, 1996; Temiz et al., 1997; Glover and Robertson, 1998; Papazachos, 1999; Mantovani et al., 2000; Hançer and Karaman, 2001; Temiz et al., 2001; Emre et al., 2003; Poisson et al., 2003a; Robertson et al., 2003; ten Veen, 2004).

both probably expressions of the NE–SW compression stress field of the Aksu regime. During the Pliocene (Fig. 10b), the centre and the south of the Isparta angle were still under the influence of the Aksu regime (Poisson et al., 2003a). In the Burdur area the biaxial NE–SW and NW–SE extension was already active (Price and Scott, 1994; Temiz et al., 1997). During this period the stress field in the study area changed from compression into extension, principally expressed by an E–W and a NE–SW extension. The E–W extension could correspond with the E–W extension responsible for the opening of the Kovada graben (cf. Glover and Robertson, 1998). The NE–SW extension, observed in the study area, can be related to the NE–SW extension in the Burdur area during Late Miocene–Pliocene (Price and Scott, 1994; Temiz et al., 1997; Glover and Robertson, 1998). In Quaternary time (Fig. 10c) the biaxial NE–SW and NW–SE extensions was still present in the Burdur area (Price and Scott, 1994; Temiz et al., 1997). Also the Isparta angle was now in extension with, during the Pleistocene, mainly an E–W extension (Price and Scott, 1994; Hançer and Karaman, 2001) and, during the Holocene, a N–S extension (Hançer and Karaman, 2001). In this period, the study area was subjected to NW–SE and NNW–SSE extension. At present (Fig. 10d) focal plane mechanisms of 20th century earthquakes in the area (Burdur, 1971; Dinar, 1995) indicate NW–SE and NE–SW oriented extension directions, respectively (Taymaz and Price, 1992; Eyidoğan and Barka, 1996).

The stress field evolution in the study area shows a transition from a dominant E–W extension to a dominant NW–SE extension. The E–W extension fits into the Kovada stress regime that dominates the apex of the Isparta angle during the Pliocene. The NW–SE extension, on the other hand, fits into the Burdur stress regime, characteristic for the NE extremity of the Fethiye–Burdur fault zone. The stress field transition in the study area thus indicates the fading influence of the Kovada stress regime and the gaining influence of the Burdur stress regime. Tectonically this may be interpreted as the incorporation of the study area in the Fethiye–Burdur fault zone, thus

reflecting a northeastwards progression of this tectonic feature. This evolution is very similar to what is observed on the SW part of the Fethiye–Burdur fault zone (ten Veen, 2004), suggesting a consistent geodynamic evolution in the entire Fethiye–Burdur fault zone.

7. Conclusion

Since the unconsolidated deposits show no kinematic indicators of fault movement, it was very difficult to unravel the neotectonic stress field evolution. Hence, these fault data were compared with the stress states that could be deduced from pre-Pliocene consolidated deposits. The lithostratigraphical relationships, the existence of superimposed slickenlines and U/Th dating of a fault-related precipitate made it possible to reconstruct the stress state history. We assume that the reconstruction of the history of stress states from a synthesis from sites all over the study area applies to the whole study area and thus reflects a changing stress field through time. This made it possible to determine the stress field evolution in this transitional zone between different tectonic domains since Late Miocene. It reveals that the area was under the influence of a transient stress regime as a result of its particular location at the extremity of different tectonic domains. In the history of the study area, a shift was observed in the origin of the main tectonic influence. In Late Miocene time, the NE–SW compression, represented by the Aksu thrust in the centre of the Isparta angle, was the dominant stress regime. During the Pliocene, compression changed into extension. It is clear that the evolving stress field through Plio-Pleistocene time indicates that the influence of the Kovada stress regime is fading and the influence of the Burdur stress regime is gaining importance, suggesting a northeastwards progression of the Fethiye–Burdur fault zone.

Acknowledgements

We thank the two anonymous reviewers for their constructive remarks and Tom Blenkinsop for the editorial review. They helped to express our views more clearly. The PhD research of Griet Verhaert is financed by the Institute for the Promotion of Innovation through Science and Technology in Flanders (IWT—Vlaanderen). This research is also supported by a Concerted Action of the Flemish Government (GOA 02/9). S. Vandycke is Research Associate of the National Research Foundation of Belgium (FNRS). M. Sintubin is Research Associate of the Onderzoeksfonds K.U.Leuven.

References

Ambraseys, N.N., Jackson, J.A., 1998. Faulting associated with historical and recent earthquakes in the Eastern Mediterranean region. Geophysical Journal International 133, 390–406.

Angelier, J., 1984. Tectonic analysis of fault slip data sets. Journal of Geophysical Research 89, 5835–5848.

Angelier, J., 1990. Inversion of field data in fault tectonics to obtain the regional stress: III. A new rapid direct inversion method by analytical means. Geophysical Journal International 103, 363–376.

Angelier, J., Bergerat, F., 1983. Systèmes de contraintes et extension intracontinentale. Bulletin des Centre de Recherches Exploration de France 7, 137–147.

Arlegui-Crespo, L.E., Simón-Gómez, J.L., 1998. Reliability of palaeostress analysis from fault striations in near multidirectional extension stress fields. Example from the Ebro Basin, Spain. Journal of Structural Geology 20, 827–840.

Armijo, R., 1977. La zone de failles de Lorca-Totana (Cordillères Bétiques, Espagne). Etude tectonique et néotectonique. Unpublished Ph.D. thesis, Université Paris VII.

Armijo, R., Carey, E., Cisternas, A., 1982. The inverse problem in microtectonics and the separation of tectonic phases. Tectonophysics 82, 145–160.

Barka, A.A., Reilinger, R., Saroglu, F., Sengör, A.M.C., 1995. The Isparta Angle: its importance in the neotectonics of the Eastern Mediterranean Region. In: Pişkin, Ö., Ergin, M., Savaşçin, M.Y., Tarcan, G. (Eds.), Proceedings of International Earth Sciences 1, Colloquium on the Aegean Region, 9–14 October 1995, Izmir-Güllük, Turkey, pp. 3–17.

Blumenthal, M.M., 1963. Le système structural du Taurus sud Anatolien. Mémoire de la Société Géologique de France 1, 611–662.

Bozkurt, E., 2001. Neotectonics of Turkey—a synthesis. Geodynamica Acta 14, 3–30.

Collins, A.S., Robertson, A.H.F., 1998. Processes of Late Cretaceous to Miocene episodic thrust-sheet translation in the Lycian Taurides, SW Turkey. Journal of the Geological Society of London 155, 759–772.

Emre, Ö., Duman, T.Y., Dogan, A., Özalp, S., Tokay, F., Kusçu, I., 2003. Surface faulting associated with the Sultandagi earthquake (Mw 6.5) of 3 February 2002, Southwestern Turkey. Seismological Research Letters 74, 382–392.

Etchecopar, A., Vasseur, G., Daignieres, M., 1981. An inverse problem in microtectonics for the determination of stress tensors from fault striation analysis. Journal of Structural Geology 3, 51–65.

Eyidoğan, H., 1988. Rates of crustal deformation in western Turkey as deduced from major earthquakes. Tectonophysics 148, 83–92.

Eyidoğan, H., Barka, A.A., 1996. The 1 October 1995 Dinar earthquake, SW Turkey. Terra Nova 8, 479–485.

Frizon de Lamotte, D., Poisson, A., Aubourg, C., Temiz, H., 1995. Chevauchments post-Tortonien vers l'ouest puis vers le sud au coeur de l'angle d'Isparta (Taurus, Turquie). Conséquences géodynamique. Bulletin de la Société Géologique de France 166, 59–67.

Glover, C., Robertson, A., 1998. Neotectonic intersection of the Aegean and Cyprus tectonic arcs: extensional and strike-slip faulting in the Isparta Angle, SW Turkey. Tectonophysics 298, 103–132.

Hançer, M., Karaman, M.E., 2001. Tectonic features of Bucak and its surroundings (southern Isparta). In: Proceedings of the Fourth International Symposium on Eastern Mediterranean Geology, 21–25 May 2001, Isparta, Turkey, pp. 33–44.

Hancock, P.L., Barka, A.A., 1987. Kinematic indicators on active normal faults in western Turkey. Journal of Structural Geology 9, 573–584.

Hancock, P.L., Kadhi, A., Barka, A.A., Bevan, T.G., 1987. Aspects of analysing brittle fractures. Annales Tectonicae 1, 5–19.

Jackson, J.A., McKenzie, D.P., 1984. Active tectonics of the Alpine–Himalayan belt between Turkey and Pakistan. Geophysical Journal of the Royal Astronomical Society 77, 185–264.

Kissel, C., Poisson, A., 1986. Etude paléomagnétique préliminaire des formations néogènes du bassin d'Antalya (Taurides occidentales, Turquie). Comptes Rendus de l'Académie des Sciences de Paris 302, 711–716.

Koral, H., 2000. Surface rupture and rupture mechanism of the October 1, 1995 ($M_w = 6.2$) Dinar earthquake, SW Turkey. Tectonophysics 327, 15–24.

Librecht, I., Paulissen, E., Verstraeten, G., Waelkens, M., 2000. Implications of environmental changes on slope evolution near Sagalassos. In: Waelkens, M., Loots, L. (Eds.), Sagalassos V, Acta Archaeologica Lovaniensia Monographiae 11, Report on the Survey and Excavation Campaigns of 1996 and 1997. University Press, Leuven, pp. 799–817.

Liesa, C.L., Lisle, R.J., 2004. Reliability of methods to separate stress tensors from heterogeneous fault-slip data. Journal of Structural Geology 26, 559–572.

Mantovani, E., Viti, M., Albarello, D., Tamburelli, C., Babbucci, D., Cenni, N., 2000. Role of kinematically induced horizontal forces in Mediterranean tectonics: insights from numerical modeling. Journal of Geodynamics 30, 287–320.

McKenzie, D.P., 1978. Active tectonism in the Alpine–Himalayan belt: the Aegean Sea and the surrounding regions (tectonics of the Aegean region). Geophysical Journal of the Royal Astronomical Society 55, 217–254.

Papazachos, C.B., 1999. Seismological and GPS evidence for the Aegean–Anatolia interaction. Geophysical Research Letters 26, 2653–2656.

Peterek, A., Schwarze, J., 2004. Architecture and Late Pliocene to recent evolution of outer-arc basins of the Hellenic subduction zone (south-central Crete, Greece). Journal of Geodynamics 38, 19–55.

Poisson, A., 1977. Recherches Géologique dans les Taurides Occidentales (Turquie). Unpublished Ph.D. thesis, Université de Paris-Sud, Orsay, France.

Poisson, A., Wernli, R., Sağular, E.K., Temiz, H., 2003a. New data concerning the age of the Aksu Thrust in the south of the Aksu Valley, Isparta Angle (SW Turkey): consequences for the Antalya Basin and the Eastern Mediterranean. Geological Journal 38, 311–327.

Poisson, A., Yağmurlu, F., Bozcu, M., Şentürk, M., 2003b. New insights on the tectonic setting and evolution of the Isparta Angle, SW Turkey. Geological Journal 38, 257–282.

Price, S.P., Scott, B., 1991. Pliocene Burdur basin, SW Turkey: tectonics, seismicity and sedimentation. Journal of the Geological Society of London 148, 345–354.

Price, S.P., Scott, B., 1994. Fault-block rotations at the edge of a zone of continental extension: southwest Turkey. Journal of Structural Geology 16, 381–392.

Ramsay, J.G., Lisle, R.J., 2000. The Techniques of Modern Structural Geology. Vol. 3: Applications of Continuum Mechanics in Structural Geology. Academic Press, San Diego, pp. 701–1061.

Robertson, A.H.F., Poisson, A., Akinci, Ö., 2003. Developments in research concerning Mesozoic–Tertiary Tethys and neotectonics in the Isparta Angle, SW Turkey. Geological Journal 38, 195–234.

Şenel, M., 1997. Türkiye Jeoloji Haritaları, Isparta Paftası (Geological Map of Turkey at 1:250,000 scale, Isparta Sheet). Mineral Research and Exploration Institute of Turkey (MTA), Publication No. 4, scale 1:250,000.

Şengör, A.M.C., Görür, N., Şaroğlu, O., 1985. Strike-slip faulting and related basin formation in zones of tectonic escape: Turkey as a case study. In: Biddle, K.T., Christie Blick, N. (Eds.), Strike-Slip Deformation, Basin Formation and Sedimentation Society of Economic Palaeontologists and Mineralogists Special Publication 37, pp. 227–264.

Sintubin, M., Muchez, Ph., Similox-Tohon, D., Verhaert, G., Paulissen, E., Waelkens, M., 2003. Seismic catastrophes at the ancient city of Sagalassos (SW Turkey) and their implications for the seismotectonics in the Burdur–Isparta area. Geological Journal 38, 359–374.

Stewart, I.S., Hancock, P.L., 1990. Brecciation and fracturing within neotectonic normal fault zones in the Aegean region. In: Knipe, R.J., Rutter, E.H. (Eds.), Deformation Mechanisms, Rheology and Tectonics Geological Society of London, Special Publication, pp. 105–112.

Stewart, I.S., Hancock, P.L., 1991. Scales of structural heterogeneity within neotectonic normal fault zones in the Aegean region. Journal of Structural Geology 13, 191–204.

Taymaz, T., Price, S., 1992. The 1971 May 12 Burdur earthquake sequence, SW Turkey: a synthesis of seismological and geological observations. Geophysical Journal International 108, 589–603.

Temiz, H., Poisson, A., Andrieux, J., Barka, A.A., 1997. Kinematics of the Plio-Quaternary Burdur–Dinar cross-fault system in SW Anatolia (Turkey). Annales Tectonica 11, 102–113.

Temiz, H., Poisson, A., Andrieux, J., 2001. The Plio-Quaternary extensional system of the western sied of the Isparta Angle in SW Turkey. In: Proceedings of the Fourth International Symposium on Eastern Mediterranean Geology, 21–25 May 2001, Isparta, Turkey, pp. 125–129.

ten Veen, J.H., 2004. Extension of Hellenic forearc shear zones in SW Turkey: the Pliocene–Quaternary deformation of the Eşen Çay Basin. Journal of Geodynamics 37, 181–204.

ten Veen, J.H., Kleinspehn, K.L., 2002. Geodynamics along an increasingly curved convergent plate margin: Late Miocene–Pleistocene Rhodes, Greece. Tectonics 21, 8-1–8-21.

Verhaert, G., Muchez, Ph., Sintubin, M., Similox-Tohon, D., Vandycke, S., Keppens, E., Hodge, E.J., Richards, D.A., 2004. Origin of palaeofluids in a normal fault setting in the Aegean region. Geofluids 4, 300–314.

Vermoere, M., Degryse, P., Vanhecke, L., Muchez, Ph., Paulissen, E., Smets, E., Waelkens, M., 1999. Pollen analysis of two travertine sections in Basköy (southwestern Turkey): implications for environmental conditions during the early Holocene. Review of Palaeobotany and Palynology 105, 93–110.

Yağmurlu, F., Savaşçın, Y., Ergün, M., 1997. Relation of alkaline volcanism and active tectonism within the evolution of the Isparta Angle, SW Turkey. Journal of Geology 105, 717–728.

Zanchi, A., Angelier, J., 1993. Seismotectonics of western Anatolia: regional stress orientation from geophysical and geological data. Tectonophysics 222, 259–274.

Zitter, T.A.C., Woodside, J.M., Mascle, J., 2003. The Anaximander Mountains: a clue to the tectonics of Southwest Anatolia. Geological Journal 38, 375–394.